Design and validation of a complete haptic system for manipulative tasks

Bergamasco M., Avizzano CA., Frisoli A., Ruffaldi E., Marcheschi S.

PERCRO, *Scuola Superiore Sant'Anna*

Abstract

The present work deals with the design, implementation and assessment of a new haptic system specifically conceived for manipulative tasks in virtual environments. Such a system has been designed by taking into account specific issues related to fine manipulation, such as multipoint haptics, coherence, transparency, and physical representation.

The haptic system herein described includes also a high performance virtual-environment engine who can manage a wide set of information and provide then to the user. This engine includes numerical algorithms for representing complex phenomenas such as: mass properties, objects weights and gravity acceleration, inter-objects collision and multifinger manipulation.

The present paper also reports a preliminary experimental validation of the achieved system. The validation procedure has been designed on the basis of the assessment procedures followed for manipulative tasks of real objects, that can be found in the scientific medical literature. According to the experiments performed, the most relevant relationships found in physical manipulation have also been confirmed in virtual manipulation. However, an in depth analysis of the results shows that several simulation parameters may also affect the features of force control during virtual manipulation.

keywords: haptic interface, virtual grasping, multipoint interaction

1 INTRODUCTION

Grasping is one of the basic haptic modes [1] and has key importance in most types of interactions between humans and the world surrounding them. Grasping an object allows us to identify some of its properties (geometric, material, and surface) [2] change its physical state (position in space, internal structure, etc.) and use it to interact with other objects.

As both [3] and [1] stated in past works, the haptic mode is dependent on the application. For example, tasks such as determining temperature, and hardness only require one point of contact. Tasks such as determining shape and size of an object are more efficient with more than one point of contact, but they can be performed with one point as well.

The nature of contact during slip provides important tactile cues regarding features on the surface as well as the nature of movement of the object, and can explain how humans take advantage of slip sensitivity when perceiving objects. Johansson and Westling conducted a series of experiments, relating tactile information to grip force when performing a lifting task [4]. They found that the ability to adjust grip force appears to be independent of the surface friction characteristics, but further studies from the same authors confirmed that this is not true for the case of objects with different curvature, and propose an active role of rotational friction for the stabilization of the grip [5].

From a psychophysical point of view, the interactions with virtual objects through multipoint interaction poses several interesting research questions at the level of sensorimotor coordination of humans. Humans un-consciously use suboptimal ([6]) algorithms for the prehension of objects when performing tasks with their hands. For instance, during a peg-in-hole task, they precisely adjust the relative position and interaction force between the peg and hole.

The same issue is of great interest even when shifted in the context of virtual environments. Simulation in virtual environments can serve as a way for assessing the performance of humans [7] and as a means for future design of the environments themselves.

Multipoint haptics [8, 9] include those devices who can simultaneously interact with the user using more than one contact point. These systems allow the representation of force and torque feedback during the simulation of dexterous manipulation and complex maneuvering of virtual objects and can improve the interaction in several applications, e.g. assembly and disassembly in virtual prototyping [10, 11], medical palpation during simulated physical examination of patients [12] and many other ones.

The existing devices at the state-of-the-art have several limitations for the simulation of grasping with more that one contact point, both in terms of workspace and mechanical interference. Furthermore, the limited amount of available devices for multifinger manipulation also slow down the development of haptic rendering modules for multiple contact points.

Non-direct contact haptics [13, 14], such as encountered haptic, who externally track the position of the human fingers, represent a promising technology for the implementation of haptics with multiple contact points. Some researchers already have developed preliminary prototypes for proofing the concept, but however, this technology seems to be still far from reaching the quality level for a satisfactory

interaction.

Manipulation by means of standard commercial haptic devices [15], commonly permanently connected to the finger through a thimble, presents five main drawbacks for the implementation of effective multipoint systems: colocation of thimbles, interference of the devices during manipulative procedures, common workspace, positional errors and time synchronization of the control procedures.

In the present work a Virtual Environment (VE) for manipulative tasks is presented. The VE system includes a novel type of interfaces and a VE engine which supports multipoint interaction and algorithms for representing several physical behaviors such as gravity, friction, mass dynamics.

The work addresses a description of the design guidelines that have been considered during the development of the mechanical system and describes the overall architecture of the VE engine. An assessment phase, designed according to existing experiments for real environment in the scientific literature, highlights results matching with existing evidences and provides further indications strictly related with the design and the setup of the parameters in the VE engine.

2 THE TWO-CONTACT POINTS HAPTIC DEVICE

The possibility of interacting with more than one point of contact is fundamental for the manipulation of objects in virtual environments. Even if almost all existing haptic interfaces provide a user interaction based on a single contact point, an increased number of contact points, not only allows to display a more natural haptic interaction [16, 17] but also improves the quality of interaction that users can perform in the environment. The haptic interface herein presented has been designed according to the following specific guidelines to enhance manipulation capabilities:

- **contact points:** to allow two or more contact points haptic interaction;
- **workplace:** to fit within a standard office desktop with minimum encumbrance;
- **workspace:** to cover a large workspace for two hands/fingers cooperative manipulation. The optimization of device encumbrance often reduces the amount workspace available at the end effector. Even if specific virtual panning and zooming exploration procedures can be set up to explore large environments [18], these constraints highly reduce the manipulation capabilities of the device;
- **force range:** to display forces typical of manipulation by hands in unstructured environments;
- **isotropy:** to achieve a isotropic behavior both under kinematic and dynamic conditions. Isotropy display of forces and inertias is more important for multipoint displays, since differences of transparency between different fingers are easily perceived;
- **other performances:** to minimize residual friction, reflected inertia and increase mechanical force bandwidth; all these factors influence the transparency of the device.

In the following the design of the haptic system according to the above guidelines is presented.

2.1 System kinematics

The system is composed of two robotic arms with equivalent RRPRRR kinematics, that provide the force-feedback for the two fingers. The user can insert his fingers in two thimbles placed on the end-effectors of both the arms, so that both single hand (thumb and index) and two hands (right and left indexes of two hands) interaction are possible. A set of rubber thimbles of different sizes allow any finger size to properly fit in the device.

Figure 1 shows the kinematics and the geometric notation that will be adopted in the following. Each arm has 6 degrees of freedom (dofs), of which the first three ones, required to track the position of the fingertip in the space, are actuated, while the last three ones, required to track its orientation, are passive. The first three dofs are kinematically equivalent to the combination of two orthogonal and incident rotational pairs and one prismatic pair, that drives a barrel along a third incident axis. The combination of these three dofs allow to position the end-effector over a large workspace. The last three

rotational pairs form a spherical wrist that allow the rotation of a sizable thimble around a common center.

The first two degrees of freedom have been actuated by means of a differential transmission composed of two capstans acting on a common driven pulley. The concurrent motion of these capstans produce a barrel rotation (link 3) along the horizontal axis z_0. The differential (opposite) motion of the capstans produce a barrel rotation along the vertical axis y_0.

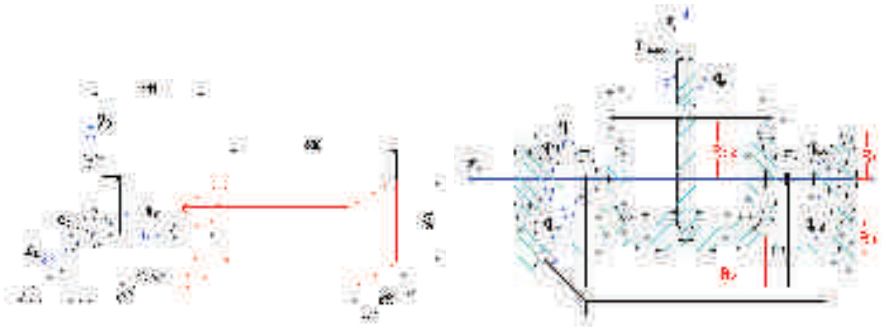

Figure 1: Kinematics of first three DOF and kinematic notation

With the nomenclature adopted in Figure 1, indicating with q_1 the tilting angle, q_2 the yaw angle, and with q_3 the displacement along the barrel axis according to Denavit Hattenberg convention, the relationships among joint and motor angles, due to the differential transmission, are given by the matrix K:

$$\begin{pmatrix} q_{m1} \\ q_{m2} \\ q_{m3} \end{pmatrix} = \begin{bmatrix} -\tau_1 & -\tau_1\tau_2 & 0 \\ \tau_1 & -\tau_1\tau_2 & 0 \\ 0 & 0 & -\tau_3 \end{bmatrix} \begin{pmatrix} q_1 \\ q_2 \\ q_3 \end{pmatrix} \tag{1}$$

where $\tau_1 = r_{c1}/r_{pm}$, $\tau_2 = r_2/r_{c2} = 1$, $\tau_3 = 1/r_b$ represent the reduction ratios, and r_b is the radius of the motor pulley that actuates the barrel axis.

This kinematic solution allows to ground the first two motors with larger bulk and thus reducing the amount of moving masses. The third motor, that provides the translational motion of the barrel, acts also as counterbalance of the barrel weight in the worst kinematic position, i.e. when the barrel is completely extended.

Once the joint angles are known, the position of the end effector can be easily computed by the direct kinematic solution:

$$\begin{cases} x &= L\cos(q_1)\cos(q_2) \\ y &= L\sin(q_1)\cos(q_2) \\ z &= -L\sin(q_2) \end{cases} \tag{2}$$

where $L = L_0 + q_3$.

The adoption of this particular kinematics with a prismatic joint combined with a differential transmission allows to combine a high kinematic isotropy performance together with a well shaped workspace. From the analysis of the device, the kinematic jacobian J can be easily found as:

$$\begin{pmatrix} \dot{x} \\ \dot{y} \\ \dot{z} \end{pmatrix} = \begin{bmatrix} -L\sin q_1 \cos q_2 & -L\cos q_1 \cos q_2 & \cos q_1 \cos q_2 \\ L\cos q_1 \cos q_2 & -L\sin q_1 \sin q_2 & \sin q_1 \cos q_2 \\ 0 & -L\cos q_2 & -\sin q_2 \end{bmatrix} \begin{pmatrix} \dot{q}_1 \\ \dot{q}_2 \\ \dot{q}_3 \end{pmatrix} \tag{3}$$

The device has been dimensioned in order to guarantee that an optimal value of the condition number of JK^{-1} was achieved all over the workspace. Figure 2 shows the variation of the condition number respectively in the plane XY and XZ of the device. In the worst case condition the device can apply a maximum continuous force of $4N$ and a maximum peak force of $10N$ applied at the end effector in all the directions.

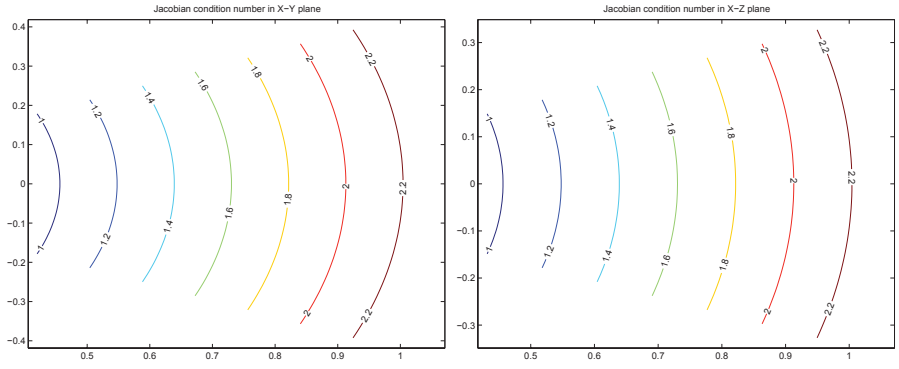

Figure 2: Contour plots of conditioning number in the two principal operating planes

2.1.1 Workspace

The dimensioning procedure also considered to guarantee a minimal workspace including a box of 300x400x600mm. The reachable workspace is given by the intersection of the two manipulator workspaces, as shown in figure 3. The geometry of the optimized workspace allows to integrate the two devices placed one in front of each other. This arrangement does not affect considerably the common reachable workspace allowing therefore the user to manipulate objects over a large space.

The mechanical interference of the structures is a further limitation occurring during the integration of several devices into the same workspace. In fact manipulation of virtual objects requires the user to free moving and rotating his hand(s). In this system the degree of interference between the two structures is reduced, and does not occur during common manipulative procedures either with one hand or two hands.

As far as the reflected mass/inertia is concerned, the use of a differential transmission systems has allowed to make the properties of the mass matrix more regular, reducing consequently the effect of Coriolis and inertia disturbances during fast motions. Specific design solution of the actuation and the transmission have been arranged to fix the transmission cables to the links, reducing the pretensioning of cables and relative friction. No reduction gear have been employed in the design, achieving therefore an almost zero backlash system. The actuation was made by low-inertia brushed DC servomotors, with

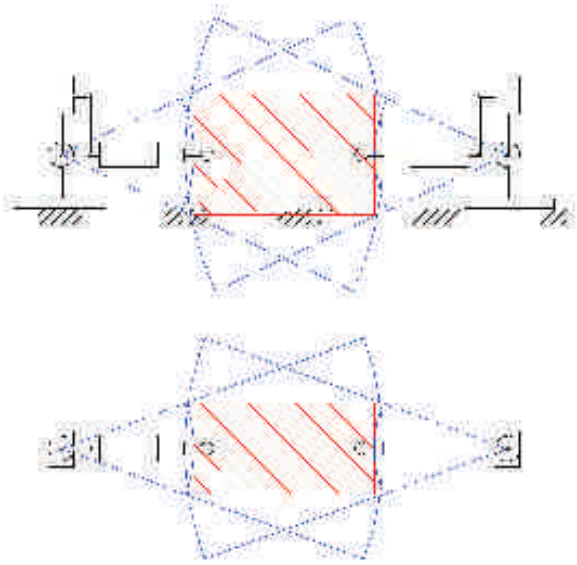

Figure 3: Workspace of two arms

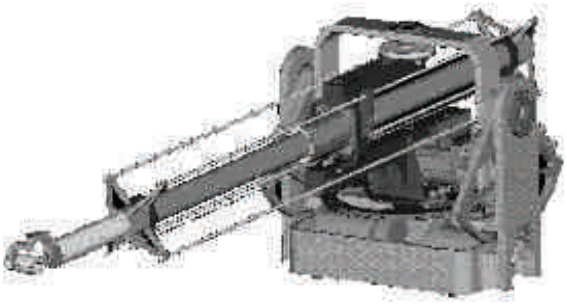

Figure 4: CAD model of the device

an iron-less construction of the rotor.

2.1.2 CHARACTERIZATION OF THE DEVICE: STATIC AND DYNAMIC RESPONSE

Stiffness was improved wherever possible. The whole structure was completely made in aluminum with some parts in carbon fiber. All fixed linkages where designed for maximizing mechanical stiffness. In order to reduce the moving mass of the barrel while preserving torsional stiffness, four additional rods were added along the barrel.

The performance of the device along the barrel axis, since it is almost aligned with the grip direction, can greatly affect the control of grip during simulation. The stiffness of the device along the barrel axis was experimentally assessed, by connecting the end-effector to an ATI nano17 force sensor, and grounding the sensor to a rigid support. The experimental stiffness estimation was found as the least square linear correlation between measured forces and displacements along the barrel axis. A value of $K_x = 23.74N\backslash mm$ ($R_{sq} = 0.994$) was found.

Also the dynamic performance of the device was experimentally assessed, by measuring the force response of the device along the barrel direction (x axis) in the same conditions as above. The input torque to the motor was a chirp input command. The force response is shown in Figure 5, and confirms that the device can reach a large dynamic bandwidth along the x direction, between 70 and 80 Hz.

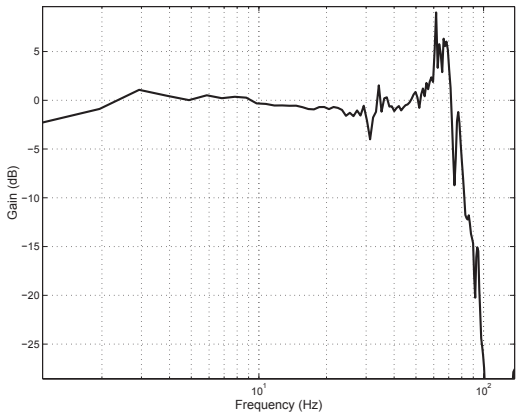

Figure 5: Dynamic force bandwidth of the device along x direction

The mechanical stiffness along the directions y and z depends instead on the extension of the barrel. The mechanical compliance along these two directions measured at the end effector is due to two main contributions:

- a linear contribution c_{lin} due to the transmission system, that can is concentrated at the level of rotational joints 1 and 2, that is mainly due to the extension of the transmission cable under tension.
- a flexional contribution c_{flex}, due to the flexion of the barrel under a flexional force

The final compliance measured at the level of the end effector, can so be expressed as

$$c_y = c_{lin} + c_{flex} = a_1 x + a_2 x^3 \tag{4}$$

The compliance c_y along the y direction was experimentally determined by fixing the end-effector of the device, applying a command torque to the motors corresponding to a force in the direction F_y, and correspondingly measuring the joint displacement through the encoder position. An interpolating cubic curve was found, representing the best least-square fit with experimental data, and is shown in figure 6. Transversal stiffness spans in the range from 1.5 to 13.5 N/mm.

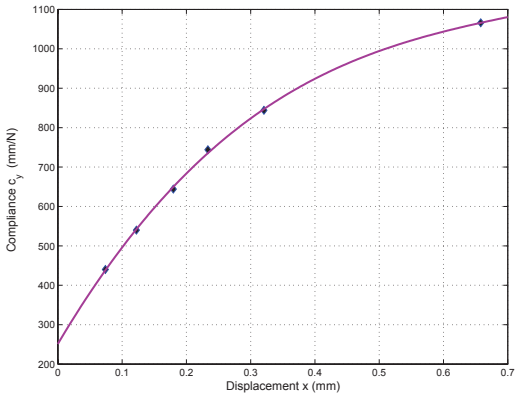

Figure 6: Experimental mechanical compliance along y as a function of barrel displacement x

2.2 Positional Error and Calibration procedures

The errors in evaluating fingers positions, in a manipulative systems may be caused by a set of factors:

- the kinematic errors related to limited encoder resolution;
- the mechanical accuracy of the manufacturing and tolerance of components;
- the relative errors among manipulators due to the position of the bases' frames.

The minimum angular rotation measured by each encoder is 1/4000 of revolution; considering the worst case in which both first two encoders update shaft position in the same time during the movement, the correspondent resolution in measuring finger position increases from 55μm to 130 μm when the barrel moves from minimal to maximal extension (L = 441 1070 mm).

System calibration procedures are implemented in order to maximize the precision in tracking finger position. It consists of two different calibration procedures.

The first one identifies the correct joint positions. It includes finding of precise markers placed on the transmission in this stage, the calibration drives the arms in a safe (for the user) and accurate manner toward a set of mechanical references.

The objective of the second calibration phase if to find the relative posture among the mechanical arms. Even having identical kinematics and being placed symmetrically on the user desktop, the fine

placement of the two HIs is left to the user which is free of adapt the device collocation in order to match the constraints of his desktop. In this case, the controller can not anymore assume that the relative position of left and right arms is a fixed pre-computed transformation matrix.

The goal of second calibration procedure is to find the exact content of this transformation matrix in terms of arms' relative position and orientation. This feature will allow to control the two different arms (placed in any relative configuration) as they would share the same coherent system of forces and position.

Once two arms are placed and fixed on desktop, a simple mechanical device should be applied on thimbles of two arms: a couple of hold fasts constrain thimbles axes to be coincident to the barrels ones and a Cardano joint is used for linking two thimbles together.

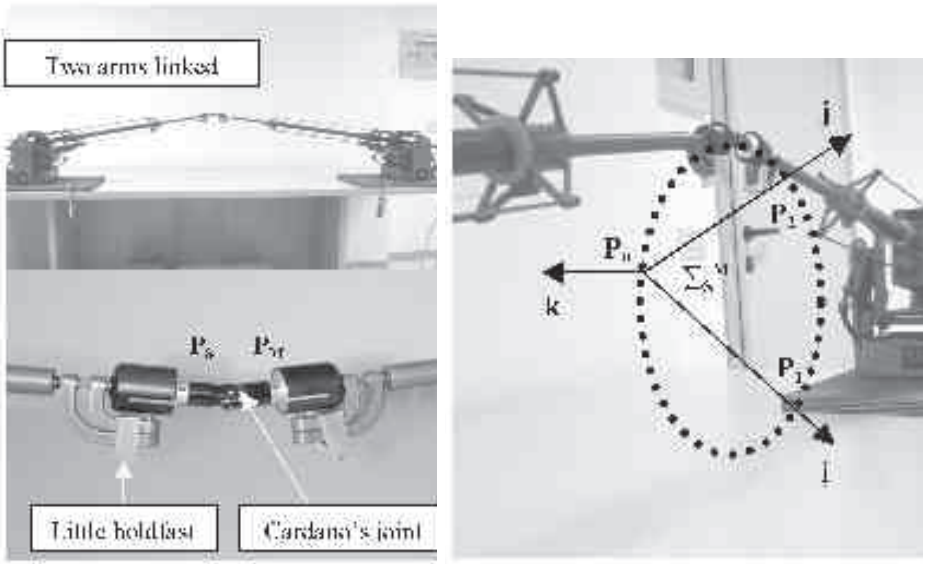

Figure 7: Mechanical set up for calibration procedure

The calibration procedure consists of moving the two arms using a positional control. In this phase one arm moves along a predefined path while the left one is force-controlled to a zero-resistance. In each frame thimbles positions are computed and recorded.

The relative base frame positions is then computed by using a set of parameters for describing their relative posture and using direct kinematic equations to identify the center of the coupling Cardano.

Using a statistical analysis over a set of samples allows the system to achieve an accuracy well beyond the sensors resolution.

It worths to mention that the procedure is independent from the specific trajectory used to find the points. Therefore even in presence of inaccurate position control the calibration procedure can provide exact calibration provided that a synchronized and accurate measure of these points is available.

3 HAPTIC RENDERING ARCHITECTURE

The VE engine implements a specific architecture for computing the force feedback to be provided during exploration and manipulation of the objects in the virtual environment. This process should provide a stable force feedback to the user which represents both all types of components in contact forces (inertia, weight, contact, friction) that may arise during exploration and manipulation tasks.

The force information for controlling the objects is determined through the position of the contact points. The position of each contact point is measured directly by the haptic interface (X_h) and the relative feedback force (F_h) is computed through a constraint-based proxy method with friction, based on [19, 20]. The haptic rendering algorithms compute the position of an additional point X_p, called proxy, lying on the object geometry, and on the basis of current X_h position and contact geometry ($\mathcal{C}$) the force is generated through a *direct rendering* method ($F_h = G(X_h, X_p(\mathcal{C}))$), using the coupling between the proxy X_p and the interface position X_h .

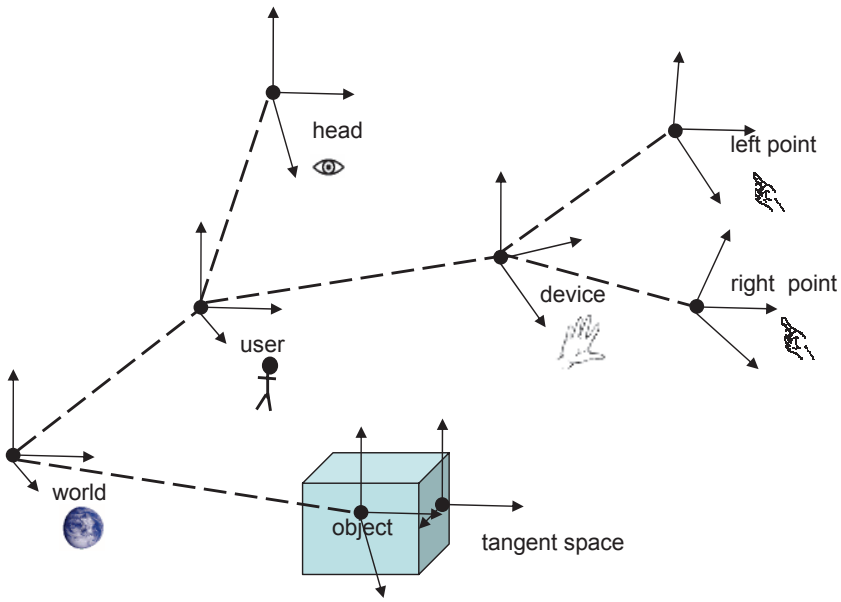

Figure 8: Reference Systems of the Haptic Rendering

A set of reference frames (shown in figure 8) has been introduced: the user frame is the main reference system that can be changed by the movements of the user in the virtual environment; attached to it there is the head frame corresponding to the position of the user's head. The haptic device has a reference system relative to the user, and every contact point position and orientation is defined according to it. Finally the last reference frame (tangent space) is defined relatively to the object and is aligned to one of its faces, and is used only by some force rendering algorithm,such as texture rendering.

3.1 GENERAL ARCHITECTURE

The basic architecture of the renderer decomposes the elements of haptic rendering in independent modules described in figure 9. Stability of the haptic response requires that the rendering process should be updated at high speed frequency (1KHz typical). It is very typical to organize simple haptic environment (without manipulation capabilities) according to a single rate process. However the complexity of features introduced into a manipulation environments require to reorganize the architecture according to a multithreaded/multirate structure. The overall architecture presented in the diagram 9 describes how components are connected by the state information, and grouped in computing threads.

There are two fundamental state information exchanged by the modules, the first is the Device State, representing all the information coming from the device, like the position of the contact points, and the other is the Object State, characterized by its reference frame in the virtual space and its properties.

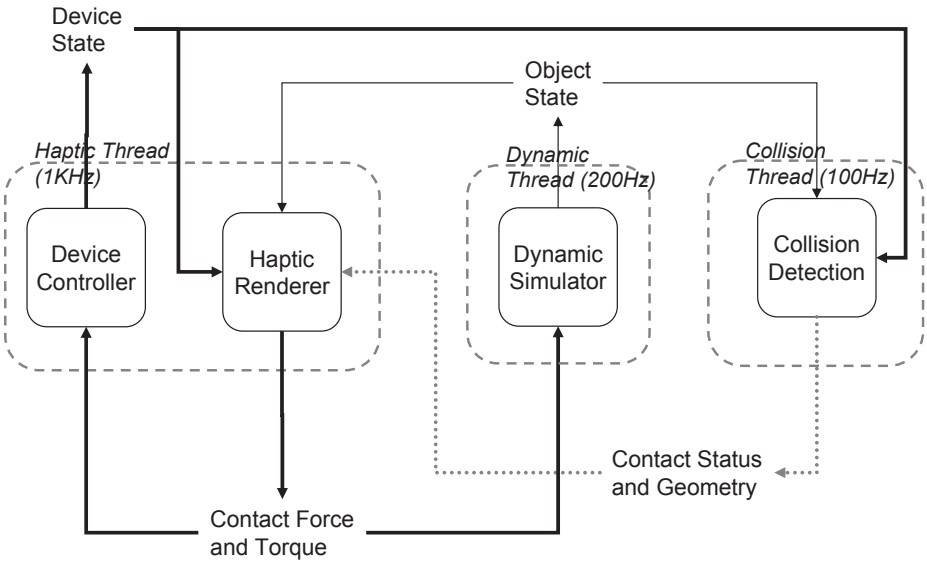

Figure 9: Haptic Rendering Architecture

The haptic rendering is performed by the Haptic Thread running at 1KHz, that receives the device information from the Device Controller and computes the contact forces in the Haptic Rendering module. The rendering itself is performed on the basis of the collision information of the haptic contact point with the object computed by the external Collision Detection component, running at a much lower rate. The collision detection computes a set of primitive that are in a volume around the contact point, and these primitives are used by the haptic renderer to compute the force feedback. The collision detection is actually implemented using an external module based on bounding volume hierarchy and running at about 100Hz.

The algorithm chosen for the haptic rendering itself is the god-algorithm, that is based on the identification of a goal point over the surface, and the constrained movement of the proxy toward this

goal point. This algorithm has been modified for taking into account a friction model that is fundamental for providing a realistic grasping of objects.

3.2 INTEGRATION WITH THE DYNAMIC ENGINE

The above description of the architecture has been extended to include also the simulation of dynamics. This feature is provided by a "Dynamic Simulator" that performs a simulation of the dynamics of the objects, and presents the state of the objects to the other components. This simulator requires a different thread, because its computation is potentially intensive, depending on the complexity of the environment and the joints between the objects. The simulation thread runs at about 200 Hz, but in prospective it could be implemented using an external Physics Processing Unit. In the actual implementation an Open Source engine called Open Dynamics Engine is used, that allows the construction of complex simulation, with different types of geometries and joints between the objects.

The objects in the complete architecture are characterized by two geometries, the first is the haptic geometry used for the collision detection with the haptic contact points and the second is the physics geometry that potentially could be simpler. This approach allows a finer haptic interaction while maintaining a smooth dynamic simulation.

The introduction of dynamic objects has two effects in the haptic renderer, the first is that the contact force exerted to the user is applied to the touched object, allowing the manipulation of the object itself. The second is that the proxy algorithm should take into account the movement of the object, in particular it is necessary to update the last proxy position with the movement of the object, that could be more correctly stated by representing the proxy in object coordinates.

It is worthwhile to analyze some stability considerations regarding the manipulation of virtual objects. Whenever an object is grasped in virtual environment by user fingers, it is virtually tied to the contact points through a couple of springs representing the virtual stiffness of the environment. In this case, the stability limits of manipulation differ from those know for the exploration of an object contour. The typical resonance frequency of this kind of contact is:

$$\frac{1}{2\pi}\sqrt{\frac{2K_s}{M_v}}$$

where K_s is the object stiffness in the virtual environment and M_v represent the virtual object mass. For the cases considered in the present work, masses ranging from $0.1 \div 0.5$ Kg and stiffness ranging from $500 \div 2000$ N/m, the typical resonance frequencies varies between $5 \div 45$Hz, well beyond the simulation frequency for the ODE components.

3.3 LINEAR FRICTION MODEL

The haptic rendering algorithm is enhanced with a linear friction model that provides additional touch realism and is fundamental for the grasping model. The standard proxy algorithm is modified with the linear friction algorithm using the friction cone model [20]: the movement of the proxy toward of the

goal is prevented by the friction itself, and perceived by the user as a tangential force. The algorithm works by building a friction cone with the top at the haptic contact point, the base centered at the god point and an aperture depending on the friction coefficient. If the last proxy position is inside the cone the proxy should not be moved and the user perceive a tangential force opposite to the moving direction, otherwise the proxy is positioned on the border of the cone. The evaluation of the position of the proxy respect to the friction cone is equivalent to decomposing the contact force in the normal and tangential components and evaluating if the tangential is greater than the normal force multiplied by the static friction coefficient. The advantage of this algorithm respect to other is only position based and it does not use a velocity estimation for the evaluation of the friction force.

The static friction is extended with the dynamic friction by using a proxy algorithm with two states, slip and not slip. During the not slip state the proxy is not moved if inside the static friction cone otherwise the state is changed to slip and the proxy moved to the border of the dynamic friction cone; when in slip mode the state is changed to not slip if the proxy is inside the dynamic cone otherwise the state is kept and the proxy moved to the border of the dynamic friction. The figure 10 shows the two friction cones and the transition diagram.

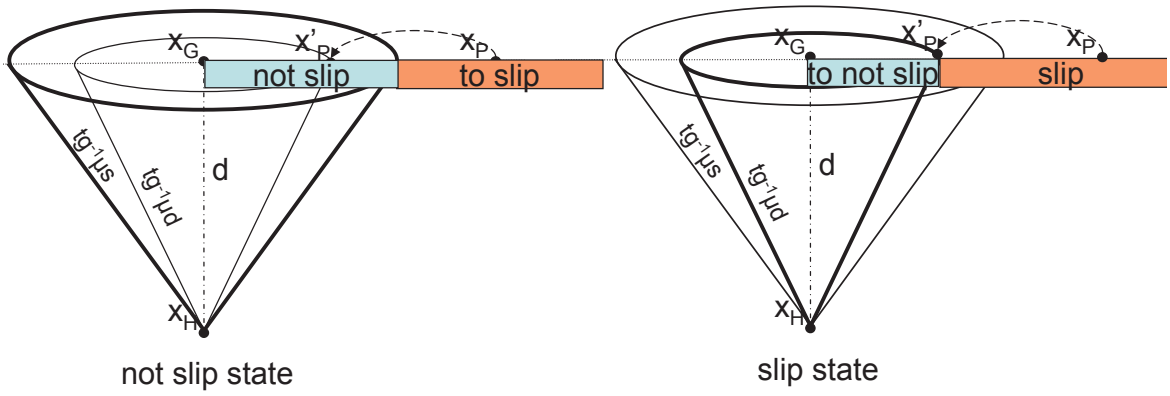

Figure 10: The linear friction cones

3.4 GRASPING MODEL

The above architecture is easily extensible to multiple contact of points: the Device Controller invokes the haptic rendering for each contact point, and the Collision Detection component performs a collision test for each contact point. From the point of view of the dynamic simulation the two contact points are invisible and they affect the simulation by applying forces on the grasped object.

The grasping of objects in this system is based on the friction and on the dynamic simulation of the objects. The grasping force exerted by the user over the object produces a friction tangential force for each of the contact points that allows to raise and manipulate the object. This model is well integrated in the dynamic simulator because when the object becomes in contact to other objects the user receives

Figure 11: Example of object grasping

a force feedback as a change of depth caused by the movement of the object. The figure 11 shows a simple example of object grasping in this system, with the display of the two contact points and the contact forces shown as the yellow vectors.

In the design phase of the grasping there are some parameters that are correlated and should be correctly evaluated for allowing a precise grasp of the object for the application, they are the static friction coefficient, the mass of the object and the stiffness of the object itself. In the evaluation part of this paper the effect of these different parameters are analyzed on a group of subjects.

Figure 12 shows the behavior of the system during the grasping of an object, with a diagram for each contact point. Three phases can be identified: the first is the lifting phase when the user starts to grasp the object, the second is the holding phase and finally there is the releasing phase when the object starts to slide. In the diagrams the green and red lines represent the position of the contact point and the object along the Y axis (aligned along the gravity vector). During the lifting and holding phases the two position have a constant difference that depends on the point of grasping over the object, then in the releasing phase they diverge because the object is falling. The black line shows the status of the friction that is zero when there is no contact, one during the non-slip state and two in the slip state: it is clear that during the lifting and holding phases the proxy is in non-slip state because it is firm between the fingers and, when the object is released, initially it changes to slip mode and then the contact is lost. Finally the blue line represents the grasping force that has an increasing and varying behavior during the lifting phase, but it is almost constant during the holding phase.

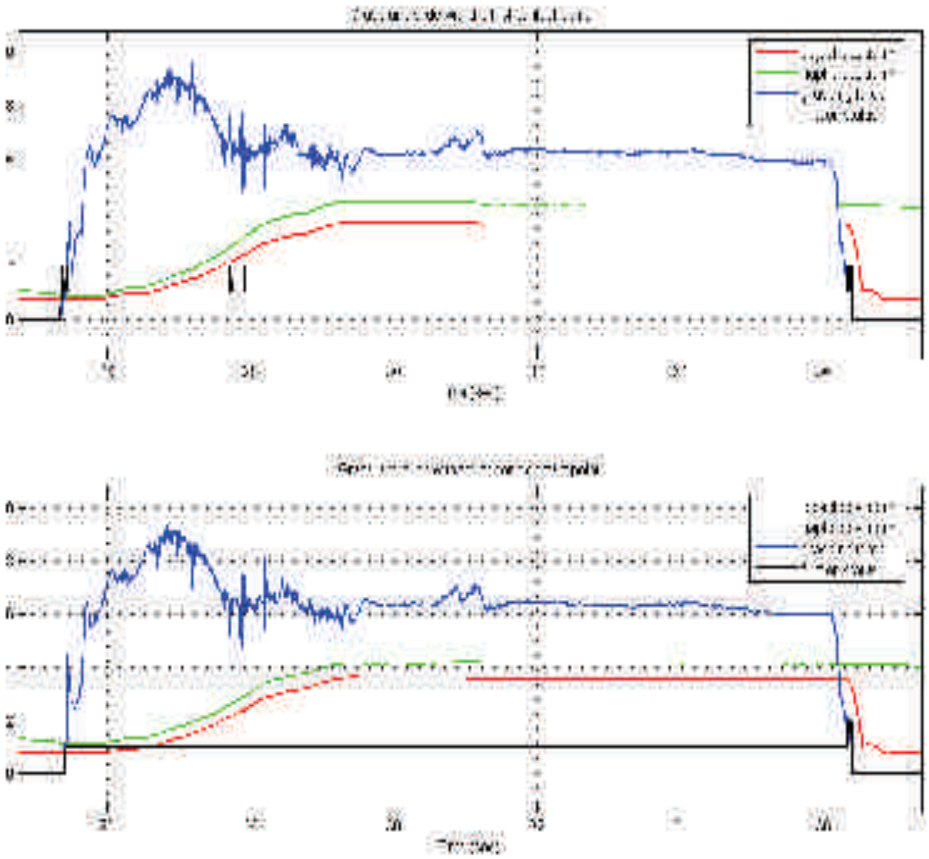

Figure 12: Forces and position during holding and release of a virtual object

3.5 AN EXAMPLE OF MANIPULATIVE APPLICATION

A preliminary application in the field of cultural heritage has been developed using the capabilities offered by the devices and the functionalities coded within the software algorithms. In this kind of application the force feedback in the manipulative task is used both to improve the attention and the realism of the interaction with the objects.

Indeed the VE system described in this article has been applied to exploit the constructivism approach, within the project CREATE (IST-2001-34231) funded by the Information Society Technologies (IST) Programme of the European Union (EU).

The aim of the application was to allow users learning the elements and the geometry of a Greek temple by reassembling it from the reconstruction of its ruins. Within this application the haptic rendering system has been integrated with an advanced visualization application, and the device has been placed inside highly immersive visualization systems (a CAVE Virtual Environment). The final system has been tested with public, and for this occasion the users were requested to manipulate ruins without any training.

The haptic rendering system was running on a personal computer connected to the device, whereas the graphic subsystem was running on a Silicon Graphic Infinity Reality. The application logic was residing over the graphic subsystem, but the dynamic of the objects was computed by the haptic rendering system. The two machines were connected by means of ethernet 100Mb/s and exchanges status informations about the objects, the device and commands.

The figure 13 shows the final graphics environment, with 3D models constructed from on-site photos.

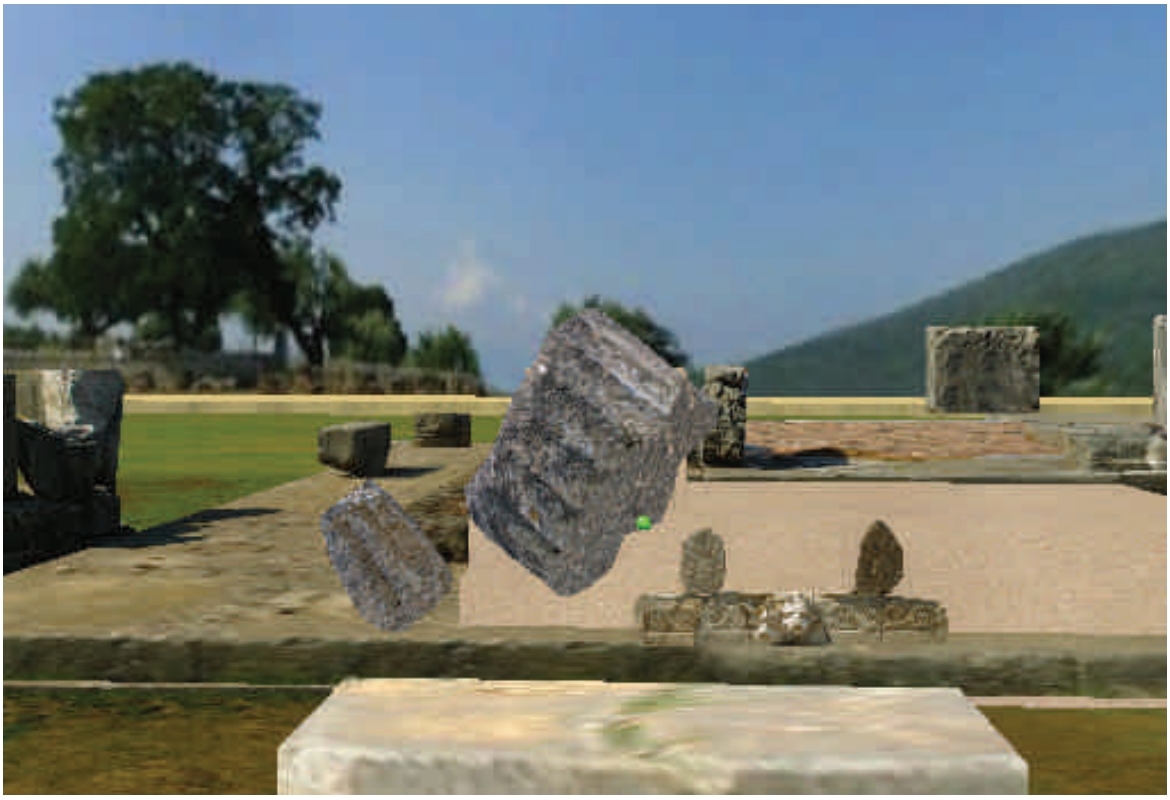

Figure 13: Object manipulation in cultural heritage

3.6 EVALUATION OF GRASPING LOAD AND SLIP FORCE IN PICK AND PLACE OPERATIONS

In order to assess the efficiency of the device and the rendering for pick and place operations, a specific evaluation was performed to compare the available data on human grasping of real objects [6, 21] with the virtual case. The influence of weight on static grip has been experimentally studied by [6], where safety margins for grasping for prevention of slipping are analyzed. The safety margin is defined as the difference between the grip force and the slip force, that is the minimum grip force required for preventing slipping.

3.6.1 Subjects and general procedures

Three healthy right-handed men, aged between 27 and 35 yrs, served as subjects for the study. The subjects sat on a height-adjustable chair. In this position the subject might held with his right hand the two thimbles connected to the haptic interfaces, and respectively wear them on the thumb and right index of his hand. A wide visualization screen was placed in front of the screen and a desktop, where during the experiment the subject was invited to place its elbow. A sequence of 27 objects was presented twice to each subject, for a total of 54 runs performed by each subject. All the objects in the randomized sequence were cubes with the same geometry, with pseudorandom changes in the weight m (0.1,0.2,0.4 Kg), in the friction coefficient, both static μ_s (0.4, 0.8, 1.2) and dynamic μ_d (0.3, 0.6, 1.1), and in the stiffness k(0.5,1, 2 N/mm). In each randomized sequence all the possible combinations of weight, friction and stiffness, without repetition, were presented to the subject. The values of μ_d were univocally associated to μ_s. The experiments were conducted with only one grasping condition, with the object hold between index and thumb tip of the same hand. Values for friction coefficients were assumed by [22] where experimental values of linear friction are reported between index tip and different materials, equal respectively to 0.42, 0.61 and 1.67 for rayon, suede and sandpaper.

3.6.2 Methods

The experiment consisted of a series of test runs. At the start of the experiment, one object with the shape of a cube was visualized at the center of scene.

Each subject was asked to grasp the object by index and thumb fingers, and to get acquainted with the weight of the object, by lifting it up and letting it falling down by continuously decreasing the gripping force.

After the necessary time to get acquainted with the object, the subject was asked to hold the object stationery in the air for 10 seconds with the minimum grasp force that he considered necessary, with the elbow leaning on the plane. When the subject was holding the object in the fixed position, both grasp F_n and friction F_t forces (respectively normal and tangential to the object surface) and positions of finger tips, object and proxies were recorded for each contact point. Statistical analysis was performed in SPSS 13.0.

3.6.3 Results

A significant correlation was found between the values of the gripping force F_n and stiffness, weight and friction values, as shown in table 1. The value of grip force F_n was found to be significantly positively correlated with mass and stiffness, while negatively with friction value. Table 1 reports the correlation coefficients obtained with a Spearmann non parametric test and significance level $p < 0.001$.

Table 1: Correlation table ($^{**}p < 0.001$).

Correlation measure	
	Grip force F_g
Friction μ_s	-0.346^{**}
Mass m	0.391^{**}
Stiffness k	0.333^{**}

Figure 14 presents several bar plots comparing the grasping force F_g in different conditions according to change in friction (top-bottom) and mass(left-right). Different colors are used for clustered bars representing the effect of stiffness in each test run.

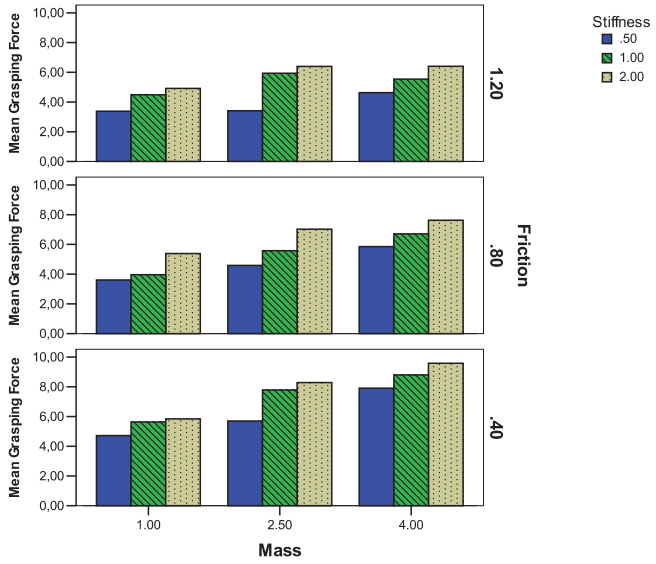

Figure 14: Mean grip force as a function of stiffness, friction and mass values

In figure 15 it is shown the change of grip force F_g vs. weight, with superimposed the error bars with confidence interval of 95%, for 9 different conditions given by different combination of friction (bottom-top) and stiffness (left-right).

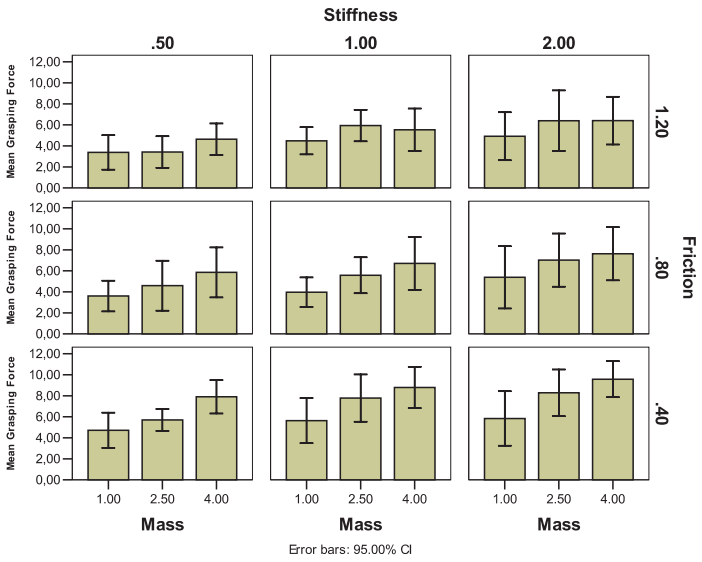

Figure 15: Mean grip force and as a function of stiffness, friction and mass values

3.6.4 Discussion

From the analysis of the results, it can be seen as greater gripper forces are required for holding heavier weights and stiffer objects, while lower gripper forces are required for higher friction values. This confirms the empirical laws that have been already found in the case of manipulation of real objects with bare fingers. In [6] it was found that the relative safety margin, defined as the safety margin in percent of the grip force, was about constant during lifting with increase of weights, was almost constant with change of weight. The calculation of the safety margin in the case of virtual manipulation allows to make an interesting comparison. As it is shown in the logarithmical plot in Figure 16 in the case of virtual manipulation, the safety margin tends to be reduced with increasing weight of the lifted mass.

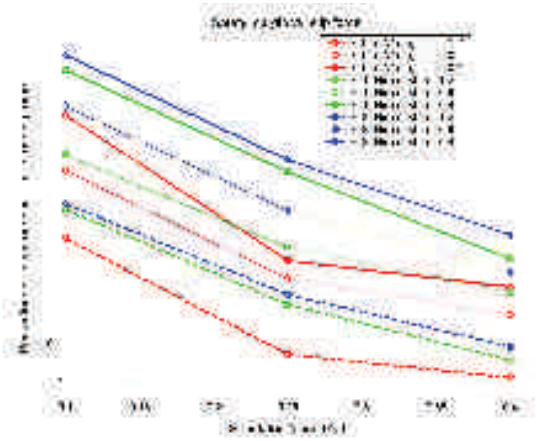

Figure 16: Relative safety margin during grasping vs. manipulated mass for different condition

This can be explained by the larger dispersion of grip forces observed for lower mass values. In fact,

due to the absence of local sensation of slip, it was more difficult to discriminate the weight of lighter objects. Moreover lighter objects required a smaller resolution in the control of force (ΔF), that is limited by the position resolution of the device ΔX, according to the law $\Delta F = k\Delta X$, where k is the simulated contact stiffness. This is confirmed by the finding that better safety margins are obtained for lower values of the stiffness, as it is evident from the plot of figure 17, where grip forces are plotted vs. slip forces. While the minimum required grip force is represented by the diagonal line, experimental data can be clustered in three main groups according to the value of contact stiffness during the simulation.

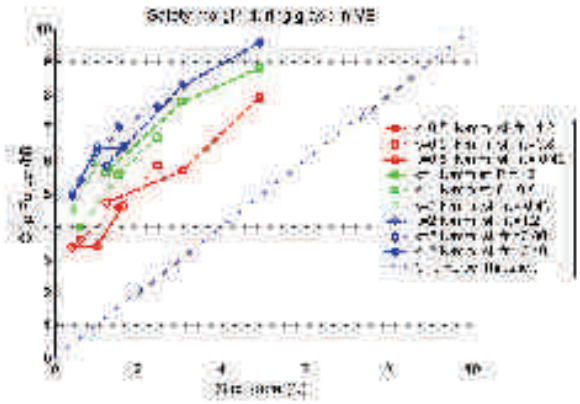

Figure 17: Grip vs. slip force, showing the relative safety margin during grasping of virtual objects

4 CONCLUSIONS

This paper has presented an haptic system for the simulation and validation of manipulative tasks in Virtual Environments. The system has been specifically designed for interaction with two contact points and integrated with an haptic rendering architecture that allow the manipulation of multiple objects. An evaluation of the performance during grasping and weight lifting, has shown that the simulation produces outcomes that are similar to experimental findings on real objects.

5 ACKNOWLEDGEMENTS

The present work has been carried out within the framework of the EU Network of Excellence ENACTIVE INTERFACES (www.enactivenetwork.org). The authors are grateful to EU who co-funded the research activities herein reported.

References

[1] Kirkpatrick A. E. Douglas S. A. Application based evaluation of haptic interfaces. In *Proceedings of the Tenth Symposium on haptic interfaces for virtual environment and teleoperator systems*, 2002.

[2] Lederman S. Hamilton C. Ramsay G. Klatzky, R. Perceiving roughness via a rigid probe: effects of exploration speed. In *Proceedings of the International Mechanical Engineering Congress, Dynamic Systems and Control Division (Haptic Interfaces for Virtual Environments and Teleoperator Systems*, volume 67, pages 27–33, 1999.

[3] R. L. Klatzky and al. Procedures for haptics object exploration vs. manipulation. In *Vision and action: The control of grasping*, pages 110–127. 1990.

[4] G. Westling R.S. Johansson. Roles of glabrous skin receptors and sensorimotor memory in automatic control of precision grip when lifting rougher or more slippery objects. *Experimental Brain Research*, 56:550–564, 1984.

[5] Per Jenmalm Antony W. Goodwin and Roland S. Johansson. Control of grip force when tilting objects: Effect of curvature of grasped surfaces and applied tangential torque. *The Journal of Neuroscience*, 18(24):10724–10734, 1998.

[6] RS Johansson G. Westling. Factors influencing the force control during precision grip. *Exp Brain Res*, 53:277–284, 1984.

[7] Yuki Ichinoo Tsuneo Yoshikawa. Impedance identification of human fingers using virtual task environment. In *Proceedings of the 2003 IEEEIRSJ Intl. Conference on Intelligent Robots and Systems*, Las Vegas. Nevada, 2003.

[8] A.; Salisbury K.; Bergamasco M.; Barbagli, F.; Frisoli. Simulating human fingers: a soft finger proxy model and algorithm. In *Proceedings. 12th International Symposium on Haptic Interfaces for Virtual Environment and Teleoperator Systems*, pages 9–17, 2004.

[9] Roman Devengenzo Federico Barbagli, Kenneth Salisbury. Toward virtual manipulation: from one point of contact to four. *Sensor Review*, 24(1), 2004.

[10] K. Puterbaugh W. McNeely and J. Troy. Six degree-offreedom haptic rendering using voxel sampling. In *Proc. of ACM SIGGRAPH*, pages 401–408, 1999.

[11] W. A. McNeely M. Wan. Quasi-static approximation for 6 degrees-of-freedom haptic rendering. *Proc. of IEEE Visualization*, pages 257–262, 2003.

[12] Tomohiro Kuroda Hiroshi Oyama Hiroyuki Yoshihara Yoshihiro Kuroda, Megumi Nakao. Shape perception with friction model for indirect touch. In *Proceedings of IEEE WorldHaptics 05*, 2005.

[13] Y. Yokokohji N. Muramori Y. Sato, T. Yoshikawa. Designing an encountered-type haptic display for multiple fingertip contacts based on the observation of human grasping behavior. In *Proceedings of the Symposium on haptic interfaces for virtual environment and teleoperator systems*, 2004.

[14] Marcheschi S. Salsedo F. Bergamasco M. Cini G., Frisoli A. A novel fingertip haptic device for display of local contact geometry. In *Proceedings of IEEE WorldHaptics*, Pisa, 2005.

[15] Thomas Debus Robert Howe and Pierre Dupont. Twice the fun: Two phantoms as a high-performance telemanipulation system. In *Proceedings of the Fourth Annual PHANTOM Users Group Workshop*, 1999.

[16] G. Jansson and L. Monaci. Haptic identification of objects with different numbers of fingers. In UNED Press, editor, *Touch, Blindness and Neuroscience*. Madrid, 2003.

[17] A. Frisoli, F. Barbagli, S-L. Wu, E. Ruffaldi, and M. Bergamasco. Comparison of multipoint contact interfaces in haptic perception. In *Workshop on Multipoint Interaction in Robotics and Virtual Reality, ICRA04*, 2004.

[18] Oussama Khatib Franois Conti. Spanning large workspaces using small haptic devices. In *First Joint Eurohaptics Conference and Symposium on Haptic Interfaces for Virtual Environment and Teleoperator Systems (WHC'05)*, 2005.

[19] C. B. Zilles and J. K. Salisbury. A constraint-based god-object method for haptic display. In *Proc. of IROS*, 1995.

[20] N. Melder and W. S. Harwin. Extending the friction cone algorithm for arbitrary polygon based haptic objects. In *HAPTICS*, pages 234–241, 2004.

[21] V. I. Johannes, M. A. Green, and C. A. Brockley. The role of the rate of application of the tangential force in determining the static friction coefficient. *Wear*, 24:381–85, 1973.

[22] J. Randall Flanagan Hiroshi Kinoshita, Lars Bckstrm and Roland S. Johansson. Tangential torque effects on the control of grip forces when holding objects with a precision grip. *J Neurophysiol*, 78:1619–1630, 1997.